Eur. Phys. J. D **24**, 197–202 (2003)
DOI: 10.1140/epjd/e2003-00175-8

THE EUROPEAN PHYSICAL JOURNAL D

Phase transformations in highly excited clusters

A. Chernomoretz and C.O. Dorso[a]

Departamento de Física Facultad de Ciencias Exactas y Naturales, Universidad de Buenos Aires, Pabellón 1 Ciudad Universitaria, 1428 Buenos Aires, Argentina

Received 10 September 2002
Published online 3 July 2003 –

Abstract. In this communication we analyze the behavior of excited drops that undergo fragmentation. We focus our attention on two scenarios: in the first one the system is free to expand, while in the second one it is confined inside a spherical volume. It is shown that the caloric curve of free expanding systems does not display a vapor branch. In the case of constrained ones, they behave as undergoing a first order phase transition at low densities while as a second order one at high densities. The transition from liquid-like to vapor-like behavior is signaled both by the caloric curves and thermal response functions.

PACS. 64.60.Qb Nucleation – 64.70.Fx Liquid-vapor transitions – 31.15.Qg Molecular dynamics and other numerical methods

1 Introduction

Since the advent of accelerators powerful enough to explore the behavior of nuclear systems at intermediate energies, a new field of research has been opened: the thermodynamics of small systems that undergo fragmentation. This problem has emerged since the first suggestion that a highly excited nuclear system might be undergoing a second order phase transition. Such hypothesis was brought up by the pioneering work of the Purdue group in which a power law was fitted to the mass spectra in collisions of highly energetic protons against heavy nuclei [1]. Since then a lot of theoretical efforts along with many experiments explored this energy range trying to characterize the occurrence of a phase transition taking place in finite systems [2–6].

In connection with this, our group has performed a series of works to disentangle the microscopic description of fragmentation process taking place in highly excited classical drops [7–9].

In this communication we explore the properties of highly excited classical drops which are either free to expand and fragment or are confined inside a spherical volume. We will show that physically meaningful fragments can be defined using stability arguments. Such a definition, when applied to expanding systems, results in the finding that fragments are formed very early in the evolution when the system is still strongly interacting. This allows us to define a time of fragment formation at which local equilibration is observed. It is then possible to define a caloric curve (CC) as the functional relationship of the system's temperature as a function of its excitation energy. We found that this CC is characterized by the fact that exhibits no vapor branch.

On the other hand, when we focus our attention at the constrained case, we find that the respective caloric curve displays a vapor branch, produced by the presence of the walls which force the system to attain global equilibrium. We show that in this case the caloric curves are strongly dependent on the density, showing for strongly diluted cases, negative specific heats. In addition, we show the resulting equation of state for such a system.

2 The model

The system that we study is composed by excited drops made up of particles interacting *via* a 6-12 Lennard Jones (LJ) potential, which reads:

$$V(r) = \begin{cases} 4\epsilon \left[\left(\frac{\sigma}{r}\right)^{12} - \left(\frac{\sigma}{r}\right)^{6} - \left(\frac{\sigma}{r_c}\right)^{12} + \left(\frac{\sigma}{r_c}\right)^{6} \right] & r \le r_c \\ 0 & r > r_c \end{cases} . \quad (1)$$

We took the cut-off radius as $r_c = 3\sigma$. Energies and distances are measured in units of the potential well (ϵ) and σ, respectively, while the unit of time used is: $t_0 = \sqrt{\sigma^2 m/48\epsilon}$. We integrated the set of classical equations of motion using the well-known Verlet algorithm [11], taking $t_{int} = 0.002 t_0$ as the integration time step. Initial conditions were constructed by cutting spherical drops of 147 particles out of an equilibrated system composed of cells with 512 particles and periodic boundary conditions [9]. Finally, the velocities of the drop particles were

[a] e-mail: codorso@df.uba.ar

slightly rescaled in order to fix the initial drop energy to the desired value.

A broad energy range was used to have the asymptotic mass spectra of the fragmented drops for the unconstrained system change from a "U shaped" pattern to an exponentially decaying one. Somewhere in between this two extremes, a power law like spectrum can be found.

In order to study the consequences of imposing a finite volume constraint to our system we used a spherical confining "wall". The considered external potential behaves like $V_{wall} \sim (r - r_{wall})^{-12}$ with a cut off distance $r_{cut} = \sigma$ where it smoothly becomes zero along with its first derivative. A rather broad range of values for r_{wall} was considered to explore the system behavior at different densities. To check the suitability of this definition we compared the results against the ones obtained with an exponentially decaying potential wall, finding no differences.

Inside this potential, a highly excited drop was initialized in the way already described, and the corresponding equations of motion were integrated. Once the transient behavior was over we performed a microcanonical sampling of particle configurations every $5t_0$ up to a final time of $140000t_0$.

3 Fragment recognition

When analyzing the free-to-expand system that undergoes fragmentation, which is a non-stationary process, the determination of the time at which fragments are formed becomes one of the key ingredients. To accomplish this task one can use a simple and intuitive cluster definition, that is based on correlations in configuration space: given a particle i and a cluster C

$$i \in C \Longleftrightarrow \exists (j \in C) \diagup |\mathbf{r}_i - \mathbf{r}_j| \leq r_{cl}$$

with r_{cl} a parameter called clusterization radius (in this work we used $r_{cl} = r_{cut} = 3\sigma$). The recognition algorithm introduced by this definition is known as minimum spanning tree (MST) fragment recognition method.

In [10] it was shown that in the analysis of the fragmentation of free expanding systems, a different recognition method, the so-called Early Cluster Recognition Algorithm (ECRA), outperforms the MST clusterization algorithm. This is so because it finds the asymptotic fragmentation pattern, in phase space, at early stages in the evolution when fragments are still not observable in configuration space. At that time the system still looks like a rather compact piece of excited matter. Instead of being defined through a proximity criteria, the ECRA fragments are associated with the set of clusters $\{C_i\}$ for which the sum of the fragment internal energies attains its minimum value:

$$\{C_i\} = \min_{\{C_i\}} \Big[E_{\{C_i\}} = \textstyle\sum_i E_{int}^{C_i} \Big]$$

$$E_{int}^{C_i} = \left[\sum_{j \in C_i} K_j^{cm} + \sum_{j,k \in C_i j \leq k} V_{j,k} \right] \qquad (2)$$

where the first sum in equation (2) is over the clusters of the partition, K_j^{cm} is the kinetic energy of particle j measured in the center of mass frame of the cluster which contains particle j, and V_{ij} stands for the inter-particle potential. We dub the partition found by ECRA as the most bound density fluctuation in phase space (MBDF), and we define as time of fragment formation (τ_{ff}) the time at which the MBDF attain microscopic stability [9]. In this way τ_{ff} is related to the time at which the system switches from a regime dominated by fragmentation to one in which the dominant decay mode is evaporation of light aggregates (mostly single particles) by the excited fragments. The ECFM-ECRA outperforms the MST not only in terms of the time at which fragments are detected but also in its capability of unveiling the nature of the fragmentation process. It shows that fragments are formed in phase space as a consequence of correlations in both q space and p space.

In order to illustrate the characteristics of ECRA against MST in a pictorial way we show in Figure 1 the result of the ECRA and MST analysis for an exploding disk of 100 LJ particles. It can be seen that the asymptotic fragments are recognized much earlier by ECRA than by MST. In this particular case the τ_{ff} corresponds to a time between the second and third panels (from left to right) while MST reaches microscopic stability at around the fourth panel.

4 Expanding systems

Once the time of fragment formation is determined, it is possible to calculate several properties of the system at fragmentation time. For this purpose the expanding system is decomposed in concentric shells and the mean radial velocity for each one of them is calculated. It has been found that the expansion is almost linear with the distance to the center of mass of the system, and that a local temperature can be defined based on the fluctuations of the velocity around the local expansive collective motion. This is so because local velocity fluctuations around the local expansion velocity are isotropic [9].

It has also been shown that, while at τ_{ff} most of the system is still interacting, the local temperature of the inner shells attain a rather constant value that can be consistently considered as the temperature of the system at fragmentation time. In this way we could calculate the corresponding caloric curve, which we define as the functional relationship between the temperature of the system at fragmentation time and the energy of the system [see Fig. 2]. It can be seen that this CC has the remarkable feature that it does not display a vapor branch but instead, after displaying a bump, it stabilizes for high energies. In the same figure we show another curve (open squares) which is proportional to the total kinetic energy (including the radial collective motion). It can be seen that the collective motion begins to be dominant at about $E = 1\varepsilon$. The presence of the expansion is responsible for the absence of a vapor branch, acting as an effective heat sink.

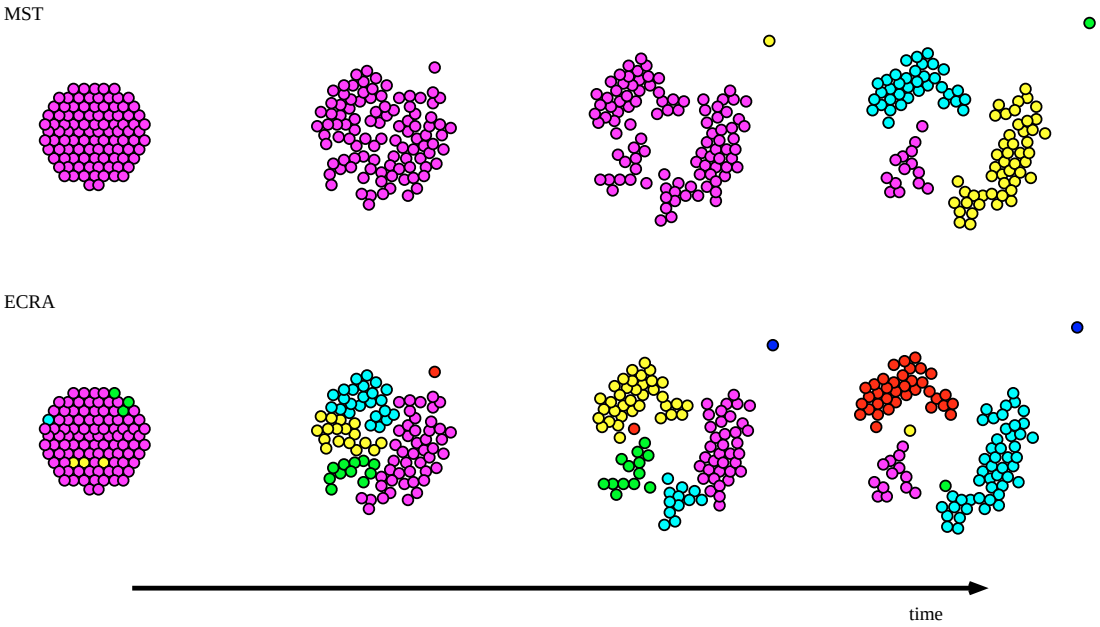

Fig. 1. In this figure, we show the results of the analysis of a given highly excited disk of 100 interacting LJ particles which undergoes fragmentation as a function of time. Different levels of gray denote clusters. The configurations displayed on top correspond to MST analysis while the ones at the bottom correspond to ECRA analysis. It can be seen that fragments are recognized by ECRA much earlier that by MST. In this particular case the time of fragment formation according to ECRA (τ_{ff}) is located between the second and third configuration displayed.

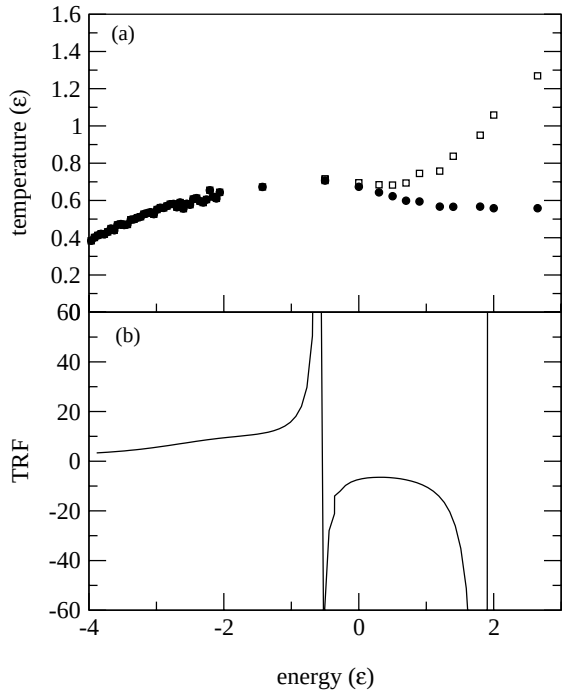

Fig. 2. In this figure, we show, in the upper panel, the caloric curve of the free to expand system (full circles) together with $\frac{2}{3}$ of the total kinetic energy per particle (open squares). The corresponding thermal response function, TRF, is shown in the lower pannel. The anomalous loop displayed by the CC induces a negative branch in the TRF. It can be seen that the system CC, calculated at fragmentation time, does not display a vapor branch. This is due to the presence of the collective motion, that becomes dominant for energies above $\sim 1.0\epsilon$.

In the lower panel we show the associated thermal response function (TRF), which is defined as:

$$TRF = \left(\frac{\partial T}{\partial E}\right)^{-1} = \left(-T^2 \frac{\partial^2 S}{\partial E^2}\right)^{-1}. \qquad (3)$$

It can be seen that this magnitude becomes negative in a region limited by two poles. The first one signals the entrance in the fragmentation regime and the second is related to the leveling off in the CC, at high energies, due to the development of the radial flux.

5 Constrained system

We now focus our attention in highly excited drops constrained inside spherical volumes. In this case the system will attain equilibrium and the MD simulation will sample the corresponding microcanonical ensemble. We will explore several observables to characterize the thermodynamical and dynamical behavior of the system. Namely, the behavior of caloric curves, specific heats, kinetic energy fluctuations and fragment mass distributions.

Due to the fact that the system is at equilibrium the temperature of the system is simply given by

$$T(E) = \frac{2}{3(N-1)} \langle K \rangle_E. \qquad (4)$$

In Figure 3 we show in the upper panel caloric curves for different densities (see caption for details). It can be

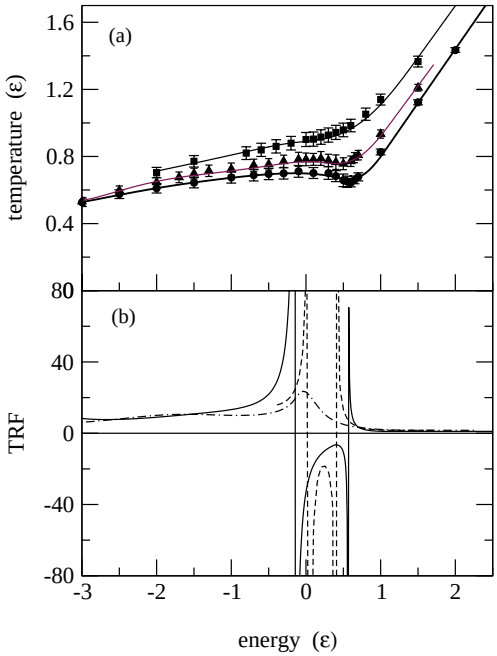

Fig. 3. In the upper panel of this figure we show caloric curves for excited 147 LJ particles contained in a spherical volume. Three densities are considered $\rho = 0.026\sigma^{-3}$ (circles), $\rho = 0.055\sigma^{-3}$ (triangles) and $\rho = 0.10\sigma^{-3}$(squares). It is seen that for the biggest constraining volume the caloric curve displays a loop. As the size of the constraining volume is reduced the caloric curve evolves into a one that only displays a change of slope. In the lower panel we show the corresponding TRF for $\rho = \sigma^{-3}$ (full line), $\rho = \sigma^{-3}$ (dotted) and $\rho = \sigma^{-3}$(dash dotted). It can be seen that the TRF attains negative values for the caloric curves that display a loop. As the density is increased the loop disappears and the TRF displays a maximum.

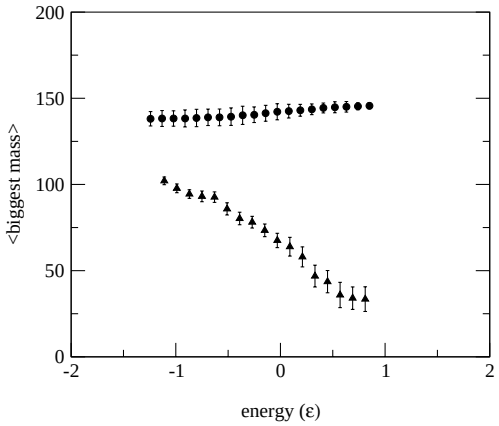

Fig. 4. In this figure we show the results of calculating the largest cluster using the MST fragment recognition algorithm for $\rho = 0.10\sigma^{-3}$ (upper curve), $\rho = 0.026\sigma^{-3}$ (lower curve). We see that at rather high densities, for which the caloric curve does not display a loop, the maximum fragment comprises most of the mass at all energies. On the other hand, when the size of the constraining volume is big enough to allow the caloric curve to display a maximum, the size of the biggest MST cluster is a decreasing function of the energy. This means that in this low density case the system fragments in well defined configurational clusters and as such, true surfaces a re formed.

immediately seen that the curves show very different behavior as a function of the size of the constraining volume. In particular at the lowest density a loop can be observed. This loop vanishes, as density is increased, and is replaced by a slope change which fades away when the density is further increased. It should be noticed that in opposition to the caloric curve for a free expanding system (Fig. 2), a linearly increasing temperature for high energies is present (this is usually referred to as the vapor branch). In the lower panel we show the associated thermal response function. It is clear that when the caloric curves displays a loop, the TRF will be characterized by the presence of a region with negative values, limited by two poles. This unusual behavior of the TRF is characteristic of non extensive systems [4,12–14]. It is also worth noticing that this behavior has also been found in the free to expand case. As the density is increased and the loop in the CC disappears, the two poles converge into a single maximum (due to finite size effects that preclude the appearance of divergences).

In order to further explore the origin of such a behavior in the caloric curve, we make use of the already described fragment recognition algorithms. In this sense we first use the MST methodology, which only takes into account spatial correlations. In Figure 4 we show the size of the maximum MST cluster as a function of the energy for two densities. It can be seen (see figure caption for details) that at densities for which the loop is not present the maximum MST cluster comprises almost all of the mass of the system. On the other hand at low densities the maximum MST cluster is a decreasing function of the energy. These two results clearly show that for that densities at which a loop can be found the system is configurationally fragmented and, as such, surfaces are formed. This is not the case when the density is high enough.

It is then of interest to explore the high density region with the ECRA methodology. When this is done a rich variety of ECRA-fragment spectra is found. In Figure 5 we show ECRA fragment spectra for $\rho = 0.1\sigma^{-3}$ and for three energies $E = -0.5, 0.0.$ and 0.9 in units of ε. We can see that, even thought there is only one MST cluster that comprises all of the mass, the displayed ECRA spectra go from "U-shaped" to exponentially decaying ones, and that in between this two extremes a power law spectra can be found. The same results can be obtained for every density, *i.e.* power laws of ECRA fragments can be obtained at all densities for a peculiar energy value that we will denote as E^*_ρ.

This feature can be further studied by extracting the corresponding critical exponents from the ECRA-mass spectra [15]. For this purpose we use the following techniques: first we assume that the fragment mass spectra is properly described by

$$n_A = q_0 A^{-\tau} f(z)$$

with A the mass of the fragment, τ a critical exponent and $f(z)$ a scaling function with $z = \epsilon A^\sigma$. ($f(z)$ has the

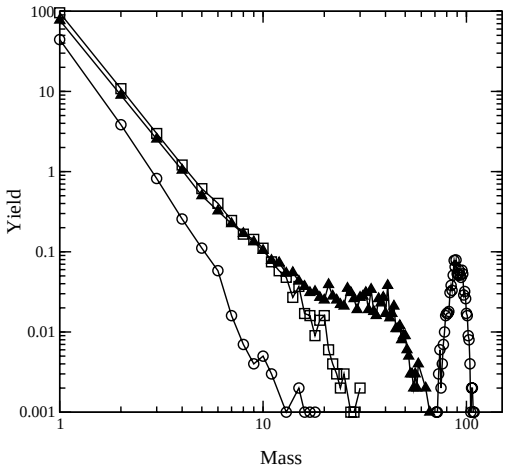

Fig. 5. In this figure, we show ECRA fragment mass spectra for a system at $\rho = 0.1\sigma^{-3}$ and at three values of the energy, namely $E = -0.5\varepsilon$ (open circles), $E = 0.0\varepsilon$ (full triangles), $E = 0.9\varepsilon$ (open squares). At this density the system forms just one cluster according to MST algorithm. But in phase space the MBDF in phase space show a rich set of patterns. In fact the ECRA fragment mass spectra go from "U-shaped" to exponentially decaying. For $E = 0.0\varepsilon$ a power law can be fitted.

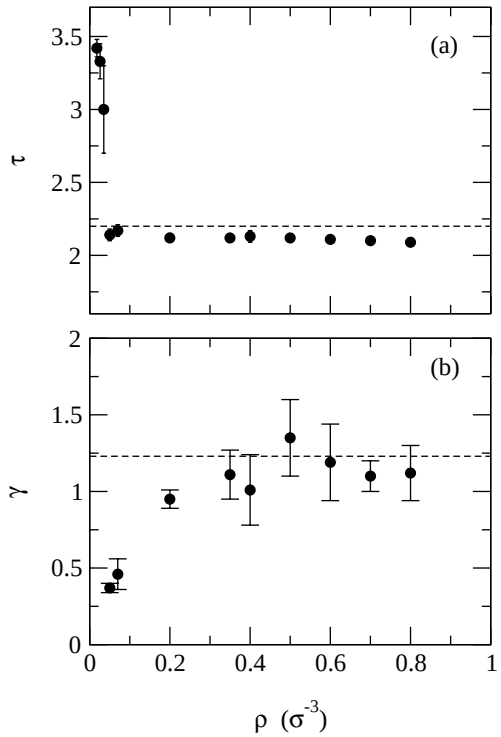

Fig. 6. In this figure, we show the values of the critical exponents τ (upper panel) and γ (lower panel). It can be seen that the first one converges to the 3D-Ising universality class (denoted by the dashed horizontal line) for densities larger than $\rho = 0.10\sigma^{-3}$, while the second does so for densities above $\rho = 0.35\sigma^{-3}$.

property that $f(0) = 1$.) On the other hand ϵ is the distance from the critical point which in this case is taken as $\epsilon = (E_c - E)$, with E the energy. Following the proposed scaling assumption, it is then immediate that at the critical point the mass spectrum follows a power law distorted by finite size effects. Moreover, it can be shown that for a "true" critical behavior, τ satisfies the following relation $2 < \tau < 3$ [16]. In order to calculate this quantity we look for that mass distribution that is best fitted by a power law once the biggest fragment has been excluded from each event. The fitting is to be done taking into account that the normalization constant q_0 is given by $q_0 = 1/\sum_A A^{1-\tau}$ [17] which means that this is a one parameter fit. The results of such a procedure are displayed in the upper panel of Figure 6. It can be seen that for densities above $\rho = 0.1$, the value of τ converges to the accepted valued for 3D-Ising universality class. We then calculate the critical exponent γ which is related to the second moment of the distribution $M_2(\epsilon) = \sum A^2 n_A \propto \Gamma_{\pm} |\epsilon|^{-\gamma}$. This calculation is performed by the methodology of "$\gamma - matching$" [17].

In this case the value of the critical energy is left as a free parameter and it is varied until the liquid and the vapor branch of the spectra are both fitted at the same time by a unique value of γ. The corresponding results for γ are displayed in the lower panel of Figure 6. We can see that γ converges to the accepted values for the 3D-Ising universality class for $\rho > 0.35\sigma^{-3}$. All these results are summarized in the following table.

At this point we can gather all the results obtained so far for the constrained system and construct the equation of state of our system. In Figure 7 we show the relation between the temperature $T(E^*_\rho)$ of the system and the density. The figure is divided in three regions, region A corresponds to the low density limit, where the caloric curve displays a loop and the calculated values of the critical exponents are far away from the ones corresponding to 3D-Ising universality class. In this region the TRF becomes negative and is limited by two poles. The strongly diluted system undergoes a first order phase transition across the $T[E^*_\rho(E)]$ line, and scale free ECRA mass distribution, found at E^*_ρ, appears as a consequence of the finite size of the system.

In region B the system has become dense enough such that the presence of internal surfaces in configurational space is severely precluded (*i.e.* the biggest MST cluster comprises almost all the mass). In this region, for each density value, the exponent τ of the ECRA-mass spectra at E^*_ρ is consistent with the one corresponding to 3D-Ising universality class. On the other hand the value of

Table 1. In this table, we summarize the main features of the thermal response functions (TRF), and critical exponents values (τ and γ) corresponding to the three density regions defined in Figure 7.

Density (σ^{-3})	TRF	τ	γ
$\rho \leq 0.05$	can be negative	$\tau > 3$	too small
$0.05 < \rho \leq 0.35$	maximum for $\rho < 0.1$	$\tau \approx 2.2$	too small
$\rho > 0.35$	no maximum	$\tau \approx 2.2$	$\gamma \approx 1.3$

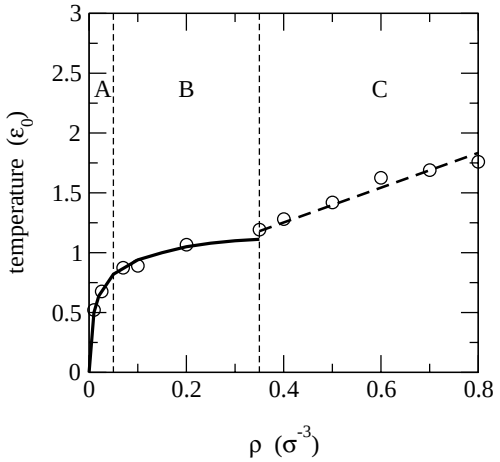

Fig. 7. In this figure, we show the resulting EOS for a constrained 147 drop of LJ particles obtained from the phase space correlation analysis. Three regions have been defined. In region A the size of the constraining volume is small enough as to allow the system to fragment in configurational space. The displayed curve corresponds to the values of T at which for a given value of ρ the best fitted power laws are found. As stated in Table 1 (see text) the critical exponents associated to this power laws are too small. In region B (intermediate densities), the system can no longer fragment in configurational space. The curve signals the region in which the best fitted power laws a found. They also correspond to the location of the maximum in the TRF (for $\rho < 0.1\sigma^{-3}$). Good values of the critical exponent τ are found. But γ exponent is too low. Finally, region C is characterized by the fact that the caloric curves are featureless (neither a loop nor a slope change were detected) In this region the best fitted power laws are characterized by good values of both τ and γ.

the corresponding γ exponent is too low. At $T(E^*_\rho)$, for $\rho < 0.1\sigma^{-3}$, the TRF attains a maximum.

Finally, in region C, at the line $T(E^*_\rho)$, both τ and γ critical exponents are consistent with the 3D-Ising universality class. In this region no maximum in the TRF could be found.

6 Conclusions

In this work we have explored the dynamical and thermodynamical properties of highly excited finite Lennard Jones clusters that undergo fragmentation. One of the main tools used all along this work is the ECFM which allows to find the most bound partition in phase space. When used in unconstrained explosive events it allows to calculate the time of fragment formation and it has been found that at this time a local equilibrium scenario is the correct one. By calculating the temperature of the system at this time we have been able to construct a CC which does not present a vapor branch but that becomes constant for high energies. In these systems the TRF attains negative values. When we extend our calculation to constrained systems, we find that the expected behavior for finite systems (nonextensive) is fulfilled, the CC display a loop and negative TRF but only for densities low enough to allow the system to develop fragments in coordinate space. As soon as the constraining volume surpasses a given threshold, the CC only displays a change of slope. By applying ECRA to the constrained configurations a novel EOS, based exclusively on morphological features of the system in phase space, can be established. According to the values obtained for the critical exponents τ and γ, three regions are recognized, low density (loop in CC, negative TRF, Power laws with "wrong" τ and γ), medium density (the CC shows a slope change, correct value of τ exponent and wrong γ exponent for the best power law fitted ECRA mass spectrum) and high density (almost featureless CC, correct values for the τ and γ exponents for the best power law fitted ECRA mass spectrum).

This work was partially supported by University of Buenos Aires (UBA) *via* grant X139. C.O. Dorso ia a member of the Carrera del Investigador (CONICET), A. Chernomoretz is a fellow of the CONICET. We thank Dr. J. Lopez for careful revision of this manuscript.

References

1. A.S. Hirsch *et al.*, Phys. Rev. C **29**, 508 (1984)
2. A. Bonsera, M. Bruno, C.O. Dorso, P.F. Mastinu, Riv. Nuovo Cim. **23**, 2 (2000); J. Lopez, C.O. Dorso, *Phase Transformations in Nuclear Matter* (World Scientific, 2000)
3. M. Moseler, J. Nordiek, Phys. Rev. B **60**, 11734 (1999)
4. D.H.E. Gross, *Microcanonical Thermodynamics* (World Scientific, 2001)
5. M. D'Agostino *et al.*, Phys. Lett. B **473**, 219 (2000)
6. F. Gobet *et al.*, Phys. Rev. Lett. **87**, 34001 (2001)
7. A. Strachan, C.O. Dorso, Phys. Rev. C **55**, 775 (1997)
8. A. Strachan, C.O. Dorso, Phys. Rev. C **58**, R632 (1998)
9. A. Strachan, C.O. Dorso, Phys. Rev. C **59**, 285 (1999)
10. C.O. Dorso, J. Randrup, Phys. Lett. B **301**, 328 (1993)
11. D. Frenkel, B. Smit, *Understanding Molecular Simulation, From Algorithms to Applications* (Academic Press, San Diego, 1996)
12. M. Schmidt *et al.*, Phys. Rev. Lett. **86**, 1191 (2001)
13. R.M. Lynden-Bell, D.J. Wales, J. Chem. Phys. **101**, 1460 (1994)
14. Ph. Chomaz, F. Gulminelli, Nucl. Phys. A **647**, 153 (1999)
15. P. Balenzuela, A. Chernomoretz, C.O. Dorso, Phys. Rev. C **66**, 024613 (2002)
16. D. Stauffer, A. Aharony, *Introduction to Percolation Theory* (Taylor and Francis, London, Washington, DC, 1992)
17. H. Nakanishi, H.E. Stanley, Phys. Rev. B **22**, 2466 (1980)